RESEARCH ARTICLE-MECHANICAL ENGINEERING

Sustainable Electrical Discharge Machining of Nimonic C263 Superalloy

Renu K. Shastri[1,2] · **Chinmaya P. Mohanty**[1] (ORCID)

Abstract

Nimonic C263, a nickel-based superalloy, finds extensive application in manufacturing of complex parts in gas turbine, aircraft and automotive industries exclusively for exhaust sections. Machining of the alloy through traditional approach is a difficult task owing to its poor thermal conductivity, work hardening and high strength properties. However, the superalloy can be machined up to desired accuracy by non-traditional machining processes like electrical discharge machining (EDM). Yet again, machining of these difficult-to-machine materials not only consumes a significant amount of energy, but also produces unpleasant noise, hindering the sustainable aspect of the process. To meet the requisite of sustainable EDM and explore the machinability, an experimental investigation is proposed in this work, when Nimonic C263 superalloy is machined with three different electrodes, viz. copper, tungsten, and copper–tungsten. Outcomes of important process parameters, viz. voltage (U), discharge current (I), pulse-on-time (T_{on}), duty factor (τ), and electrode material, are studied on the responses, viz. specific energy consumption, machining noise (N), material removal rate, electrode wear rate, surface roughness (R_a) and radial overcut (C). Analysis of variance is conducted to analyse the influence of each parameter on the responses. A scanning electron microscope investigation is carried out to analyse the pre-machining and post-machining scenarios on the machined surface. The multiple responses are converted into single response by calculating the net outranking flow by application of preference ranking organization method for enrichment evaluation (PROMETHEE) approach. The PROMITHEE-based results are further improved by using a hybrid cuckoo search algorithm (combined PROMITHEE-based cuckoo search). A confirmative test is further conducted on the optimum machining conditions obtained by the hybrid approach (combination of PROMITHEE and cuckoo search) indicating an overall improvement of 6.02% for the responses, validating the proposed work.

Keywords EDM · Nimonic C263 · SEC · Machining noise

1 Introduction

Nickel-based superalloys, composites and various difficult-to-cut materials can be precisely cut into intricate shapes by non-traditional machining operation like electrical discharge machining (EDM). Nowadays the process contributes a prime share in production of complex parts in aerospace, automotive, tool, die and various surgical instruments manufacturing industries [1, 2]. The technological advancement of the process has even led to the accurate machining of non-conducting and low conductive materials, viz. composites, ceramics, and glasses [2]. The spark erosion process primarily uses thermal energy, to remove material from the work surface by series of spark discharges occurring in between the electrodes. The process is completed within an immersed dielectric medium, when a constant energy source is supplied in between the tool and workpiece that produces conductive plasma channel as the positive ions and electrons interact. Occurrence continuous of spark discharges causes melting and vaporization of material from both the electrodes and the melted debris are flushed away from the work surface by the flushing action of dielectric fluid. Generally, a temperature of the range 8000–12,000 °C is produced on the machining zone leaving behind the impression of the

✉ Chinmaya P. Mohanty
   chinmaymohantymech@gmail.com

1 School of Mechanical Engineering, Vellore Institute of Technology, VIT University, Vellore, Tamil Nadu 632014, India

2 School of Mechanical and Civil Engineering, MIT Academy of Engineering, Alandi, Pune 412105, India

electrode on the work surface after dielectric flushing. As the process is primarily used to machine low conductive and hard materials, the required energy consumptions for melting and vaporization of the electrodes are very high. This in turn directly governs the cost of manufacturing thereby enhancing the unit price per product. Along with high energy consumption, the machining noise plays an important role to decline the productivity of the process by creating unpleasant, harmful mechanical vibration, which negatively affects the tool engineers' concentration and performance during machining. Therefore, to ensure productivity these two characteristics along with other machining performances are the important aspects in the context of sustainable machining operation.

Sustainable manufacturing can be defined as the process which aims at manufacturing of product through a process that conserves minimum energy, reduces negative environmental influences, economically sound and safe for employees, and buyers [3]. Thus, energy consumption and environmental impact are considered to be the most critical parameters to achieve sustainable manufacturing. In this context, several studies reported are discussed below. Zhang et al. [3] attempted to optimize energy consumption, machining noise, carbon emission along with other machining characteristics, viz. material removal rate (MRR) and electrode wear ratio (EWR) while machining Ti6Al4V workpiece with copper and graphite electrode. Ming et al. [4] have compared the conventional and magnetic field-assisted EDM performance to achieve sustainable machining operation. They concluded that magnetic field effect increases material erosion efficiency, energy utilization efficiency and material removal rate. Li et al. [5] proposed an empirical model to predict energy consumption with accuracy up to 90 percentages. Bagaber et al. [6] studied the power consumption in dry turning of stainless steel with an uncoated carbide tool. The study reported the minimum power consumption under dry conditions. Zhang et al. [7] applied a microcrack wire electrode to improve the machining characteristics of thin-wall component during sustainable wire cut operation. Franco et al. [8] studied the energy consumption in micro-drilling process. Dong et al. [9] suggested water in oil nano-emulsion dielectric fluid can enhance the machining performance while machining SKD61 workpiece with tubular graphite electrode. They reported increase in MRR and decrease in EWR by using nano-emulsion dielectric fluid during a sustainable machining approach. Singh et al. [10] suggested various sustainable approaches for environment friendly EDM.

Along with these sustainable machining approaches, several studies reported machinability investigation on numerous alloys, superalloys and composites etc. In this direction, various studies reported are discussed below. Torres et al. [11] reported that discharge current was the most dominant

parameter when Inconel 718 is machined in EDM process. Lee et al. [12] studied the machinability of tungsten carbide with copper–tungsten electrode. Rahul et al. [13] studied the surface characteristics of Inconel 718 while machining with copper electrode. Mohanty et al. [14] investigated the machinability of Inconel 718 in EDM with various electrode materials like graphite, brass and copper. Finally, the optimum parametric setting is found by using quantum behaved particle swarm optimization (QPSO) algorithm. Rajesh et al. [1] have studied the machinability of Inconel 718 alloy with a tubular copper electrode. They concluded that pulse current is highly influential factor for tool wear, recast layer and crack propagation. Tai et al. [15] have observed increase in pulse current and decrease in pulse time duration can lead to reduction in cracks occurring on the machined surface. Bhaumik et al. [16] investigated the influence of process parameters and electrode material on surface integrity and radial overcut while machining of Ti–6Al-5 workpiece. Mohanty et al. [17] conducted experiments on Inconel 825 workpiece and determined the optimum parametric setting to achieve the best results. Ming et al. [18] reported the challenges of machining of advanced ceramic materials with EDM. Additionally, several studies reported some technological modifications with the experimental set-up to improve the machining efficiency of the process. In this direction, few studies reported presence of suspended powder particles can enhance the EDM performance [19–22]. Numerous studies reported cryogenic treatment to tool and workpiece can boost machining performance [23–26]. Srivastava and Pandey [27] studied the machining performance of the cermet electrode and conventional copper electrode in ultrasonic-assisted cryogenically cooled EDM (UACEDM). Furthermore, few studies reported the effect of different dielectrics on machining performance of EDM [28–30].

In recent years, various researchers have opted for using multi-criteria decision making (MCDM) tools and artificial intelligence (AI) approaches to achieve the optimum machining conditions. In this context, Bose et al. [31] have used grey relation analysis techniques to optimize the multiple performances, viz. MRR, surface roughness and overcut of EDM process. Dewangan et al. [32] have studied the surface integrity of AISI P20 workpiece and used grey-fuzzy logic approach to get the optimum parameters. Saravanan et al. [33] used cuckoo search algorithm to optimize the wire cut EDM parameters. Multi-objective particle swarm optimization (MOPSO) algorithm is used to achieve the optimum machining condition [34, 35]. Jung et al. [36] have attempted to optimize the EDM parameters using Taguchi and grey relation analysis. Majumdar et al. [37] have compared desirability-based multi-objective PSO algorithms and found desirability-based multi-objective PSO-constriction factor is the most significant algorithm for finding the optimum parameters. Mohan et al.

[38] used genetic algorithm to find optimum parameters in rotary EDM of SiC/6025 Al composite. Sahu et al. [39] proposed an artificial neural network (ANN)-based model in combination of non-dominated sorting genetic algorithm (NSGA-II) to optimize the process parameters to attain enhanced MRR and reduced tool wear rate (TWR).

In spite of significant research reported on various nickel-based superalloys, to study the machinability, several unique work materials still exist, upon which investigation is yet to be carried out on serious note. Nimonic C263 superalloy is one of such materials which finds extensive applications in manufacturing, exhaust section components in aerospace, gas turbine, nuclear reactor, automotive, biomedical, marine, chemical industries owing to high hardness and excellent temperature resistant abilities. The material is suitable for high strength and high-temperature applications as it an alloy of nickel, chromium, cobalt, molybdenum along with presence of elements, viz. tungsten, niobium etc. The alloy possesses poor thermal conductivity along with high creep resistance, corrosion resistant, high-stress rupture strength and high-temperature oxidation resistance properties [40–42]. These excellent properties along with poor thermal diffusivity make the material difficult to machine by conventional machining approach [43, 44]. However, the material can be machined with ease by non-conventional machining process like EDM. Few studies reported investigations on the machinability of the superalloy have been discussed below. Mandal et al. [40] studied the micro-hardness, residual stress, surface roughness, surface morphology and elemental composition of the wire-electric discharge machined surface of the Nimonic C263 alloy by rough cut and finished cut strategies. Rao et al. [41] adopted particle swarm optimization (PSO) and response surface design methods (RSM) to achieve the optimum level of machining parameters. Shastri and Mohanty [42] studied the effect of process parameters on MRR and surface roughness while machining Nimonic C263 workpiece with various electrodes like copper, copper–tungsten and tungsten.

Extensive study of past literature pertaining to the machinability studies of the EDM process; it is evident that mostly researchers have focused on workpieces such as various grades of Titanium, Inconel, Tool steel, Composites. Limited numbers of attempts have been reported to explore the machinability of Nimonic C263 workpiece [40–42]. There is also hardly any evidence on sustainable machining measures, viz. energy consumption during machining, machining noise, while machining a low conductive material like Nimonic C263. Keeping an eye on the ever-increasing demand, extensive applications of the workpiece and sustainable machining environment, the machinability investigation of the superalloy with a variety of electrodes holds immense significance.

In view of this, the prime objective of this work is to explore the machinability of Nimonic C263 workpiece, meeting the demand of sustainable machining approach, with variety of electrodes, viz. copper, tungsten, and copper–tungsten etc. Outcomes of important process parameters, viz. voltage (U), discharge current (I), pulse-on-time (T_{on}), duty factor (τ), and electrode material on the responses, viz. specific energy consumption (SEC), machining noise (N), material removal rate (MRR), electrode wear rate (EWR), surface roughness (R_a) and radial overcut (C), are investigated through justifications and analysis. A scanning electron microscope (SEM) study is conducted to evaluate the pre-machining and post-machining changes of the machined surface of the workpiece. A preference ranking organization method for enrichment evaluation (PROMITHEE) is used to find the best ranked result from the multiple responses by calculating the outranking flow. The approach is simple, easy for calculation and is implemented successfully by many researchers to solve problems of various domains [45–49]. The best result obtained by the PROMETHEE approach is further improved by application a cuckoo search (CS) algorithm to establish a novel hybrid optimization framework (PROMITHEE-based cuckoo search) to achieve the optimum machining conditions. The algorithm is simple, easy for implementation and effectively used for solving many engineering problems [50–53]. The optimum machining condition is validated by conducting a confirmative test predicting significant improvement for each of the responses.

2 PROMETHEE Approach

The performance measures of EDM require critical decision-making thoughts due to the involvement of contradictory responses, viz. MRR, EWR, surface roughness etc. Hence, to ensure productivity of the process, robust selection of process parameters is vital. In this context, MCDM approaches are found be the most effective tool to explicitly handle multiple contradicting responses. Therefore, to make the decision-making process simpler, PROMITHEE method is used to select the best alternative from the experimental runs in this work. The method is user simple, user-friendly for outranking and is extensive used for solving numerous to real-life planning problems [45–49]. The method involves the following steps:

Step 1 At first, the attributes for the considered decision-making problem are chosen and the decision matrix is formed by finding the attributes satisfying the requirements. SEC, machining noise, MRR, EWR, surface roughness and radial overcut are taken as six selection criteria in this work. MRR is considered as beneficial criteria while SEC, machining noise, EWR, surface

roughness and radial overcut are taken as non-beneficial criteria.

Step 2 After forming the decision matrix, the relative importance of each selection criteria is determined relating to the requirements of our objective. Based on the scale of relative importance, pairwise comparison matrix is created. When criterion is compared to itself, it always gives value 1. Thus, the diagonal of the matrix is assigned values 1 in the pairwise comparison matrix. 3, 5, 7, and 9 correspond to the moderate importance, strong importance, very strong importance, and absolute importance (with 2, 4, 6, and 8 for a compromise between the previous values).

Step 3 After forming the pairwise comparison matrix or preference matrix, each criterion's relative normalized weight is determined by calculating the geometric mean of the ith row of the matrix and a normalizing the geometric means of rows in the comparison matrix. The geometric mean is calculated by following Eq. 1.

$$\mathrm{GM}_i = \left\{ \prod_{j=1}^{M} r_{ij} \right\}^{1/M} \tag{1}$$

where M represents criteria, r_{ij} denotes the comparative importance of criterion i with respect to criterion j. In the formed matrix, $r_{ij} = 1$ when $i = j$ and $r_{ij} = 1/r_{ij}$. GM_i represents the geometric mean of ith row in the matrix. The normalized weight is calculated by using Eq. 2:

$$W_i = \mathrm{GM}_i \bigg/ \sum \prod_{j=1}^{M} \mathrm{GM}_i \tag{2}$$

where W_i denotes the relative normalized weight.
Table 1 shows the preference matrix of attributes with geometric mean and normalized weight. To find a relative normalized weight for each criterion, this geometric mean method of AHP has been used in this study. AHP method is simple and used to reduce the inconsistency in judgments. The summation of all weights of decision criteria is 1 that is ($\Sigma W_i = 1$) [48].

Step 4 After finding the weights using the AHP method, the preference function is developed for each criterion.

Table 2 Process parameters and their levels

Process parameters	Unit	Symbols	Levels		
			− 1	0	1
Discharge current (I)	A	A	3	5	7
Voltage (U)	V	B	50	60	70
Pulse on time (T_{on})	μs	C	100	200	300
Duty factor (τ)	%	D	80	85	90
Electrode		E	Tungsten	Copper tungsten	Copper

This preference function represents the function of the difference between evaluations and is shown in Eq. 3.

$$P_{i(a,b)} = F_i\big[d_i(a,b)\big], 0 \le P_{i(a,b)} \le 1 \tag{3}$$

where $d_i(a, b)$ represents the difference between the two alternatives (a and b). F_i represents the non-decreasing function. The preference is set to 0 when the deviations are negative. For non-beneficial criteria where the lower values are required, the preference function is rewritten as follows:

$$P_{i(a,b)} = F_i\big[-d_i(a,b)\big] \tag{4}$$

Step 5 The overall performance index π (a, b) is determined by following formula

$$\pi_{(a,b)} = \Sigma P_{i(a,b)} W_i \tag{5}$$

where $P_i(a, b)$ demonstrates preference function, and W_i represents weights assigned to each criterion.

Step 6 The leaving flow, entering flow and the net outranking flow for different alternatives are calculated by Eqs. 6, 7 and 8. For each pair of criteria in the decision matrix, the values of $\pi_{(a, b)}$ and $\pi_{(b, a)}$ are determined.

The leaving flow is given by

$$\emptyset^+(a) = \sum_{b=1} \pi_{(a,b)} \tag{6}$$

Table 1 Preference matrix with GM and Normalized weight

	MRR	EWR	SEC	R_a	N	C	GM	Normalized weight
MRR	1	3	3	3	5	5	2.9489	0.3863
EWR	1/3	1	3	3	3	3	1.7253	0.2260
SEC	1/3	1/3	1	3	3	5	1.3019	0.1705
R_a	1/3	1/3	1/3	1	3	2	0.7751	0.1015
N	1/5	1/3	1/3	1/3	1	2	0.4944	0.0648
C	1/5	1/3	1/5	1/2	1/2	1	0.3873	0.0509
						Sum	7.6329	1

Table 3 Chemical composition of Nimonic C263 obtained through EDS analysis

Elements	Ni	Co	Cr	Mo	Ti	Al	V
Weight%	48.98	18.14	13.39	7.38	1.22	0.65	0.27

The entering flow is given by

$$\emptyset^-(a) = \sum_{b=1} \pi_{(b,a)} \tag{7}$$

In the above equations, $\pi_{(a,\,b)}$ and $\pi_{(b,\,a)}$ represent the preference functions.

The net outranking flow is given by

$$\emptyset(a) = \emptyset^+(a) - \emptyset^-(a) \tag{8}$$

The alternatives are ranked according to the net outranking flow values. Bigger is the net outranking flow value better is the alternative. The proposed PROMETHEE method provides a complete ranking of alternatives form best to worst with the help of net outranking flow.

3 Experimental Design and Procedure

3.1 Experimentation Planning

The experimental architecture is planned as per Box–Behnken design of response surface methodology (RSM) in order to extract maximum information from the study. From the extensive literature review discharge
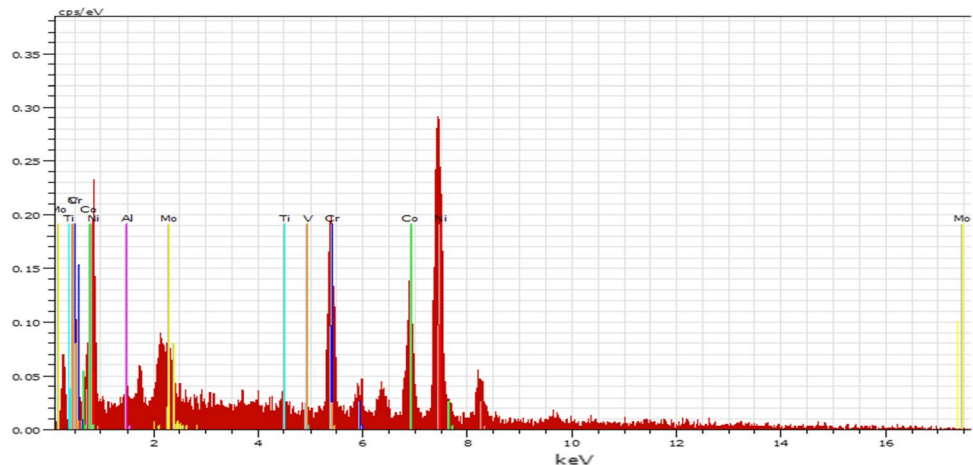
current (I), voltage (U), pulse-on-time (T_{on}), duty factor (τ) and electrode material are identified as the important process parameters and hence decided to study their effects on responses, viz. SEC, machining noise (N), MRR, EWR, surface roughness (R_a), and radial overcut (C) [3, 14]. The process parameters along with their symbols and levels are furnished in Table 2. Each parameter is varied at three levels during the experiments.

Commercially available, Nimonic C263 plates of dimension $(100 \times 100 \times 5)$ mm^3 are brought for the investigation. Shortly after purchase the plates are subjected to energy-dispersive spectrometry (EDS) analysis for sample confirmation. Table 3 shows the chemical composition obtained through the analysis, and Table 4 represents the thermo-mechanical properties of the Nimonic C263, which have been reported by Ezilarasan and Velayudham [54].

Figure 1 represents the EDS analysis of Nimonic C263 alloy for proper identification of the workpiece. From the analysis, clear visual of presence of sharp peaks for the elements such as Ni (high content), Cr, Co, Al, Mo, Ti, and V can be seen indicating the pure nature of the alloy. The peak also matches with the peak reported by the previous researchers Ezilarasan et al. [55]. The electrode materials used for experimentation are tungsten, copper–tungsten, and copper, respectively. For suitability during machining, the electrodes are reduced to 150 mm length and 10 mm machining diameter. The thermal conductivity of tungsten, copper–tungsten and copper is 173, 182 and 385 W/mk, respectively.

Die sinking ZNC EDM setup (make: Electronica, Pvt. Ltd India) is used to conduct the experiments which is shown (Fig. 2b). In this conventional EDM set up, Kerosene is used as a dielectric fluid due to its favourable machinability

Table 4 Thermo-mechanical properties of Nimonic C263 [54]

Property	Density	Poisson's ratio	Thermal conductivity	Heat capacity	Specific heat
Value	8360 kg/ m^3	0.3	11.72 W/m K	0.461 J/g °C	461 J/ kg °C

Fig. 1 EDS analysis representing elemental composition of Nimonic C263

properties, viz. excellent flushing ability, good dielectric strength, low viscosity, low specific gravity and ease of access reported by researchers [56–63]. This usage is further supported by previously reported sustainable and green EDM works [64–66]. Each experiment is conducted for 10 min. The EDM experimental setup along with its accessories such as energy meter (Fig. 2a) and sound level meter (Fig. 2c) are shown Fig. 2. Figure 3 shows the Nimonic C263 workpiece with three electrodes.

3.2 Calculation of Performance Measures

3.2.1 Calculation of Specific Energy Consumption (SEC)

The EDM machine has a three-phase power supply arrangement to consume energy and perform machining. To measure the energy consumed during machining, three voltage wires are connected to the input terminal of voltage form three-phase arrangement. Further, they are clamped with the correct direction of the clamp sensor to the electric wires in an appropriate wire depending up on their wiring number. The energy consumed during EDM recorded by a Multimeter Model number-CPEM-07 is shown in Fig. 2a. After precise connection of all the wires to the machine, the instrument is started and the function switch of the Multimeter CPEM-07 is turned on to indicate the energy consumed in Watt (W). Energy consumed during each experiment is detected for 5 min so as to calculate the energy change within this period. After this, average of all values is calculated. Based on previously reported works, the SEC is calculated [3, 5, 7, 8] by using Eq. 9.

$$SEC = \frac{Energy\ consumed\ (E)}{Volume\ of\ removed\ material\ (V)} \tag{9}$$

Here, the energy consumed is calculated by Eq. 10, and the volume of material removed per unit time is called material removal rate (MRR). The calculation of MRR is reported in Sect. 3.2.3.

$$Energy\ consumed\ (E) = I \times U \times T_{on} \tag{10}$$

3.2.2 Calculation of Machining Noise (N)

For measuring the machining noise, a sound level meter digital noise meter Pixel GM1351 is shown in Fig. 2c. To avoid the undesirable disturbances and record the utmost pure quality frequencies, other laboratory instruments are turned off in an isolated machining set-up during the

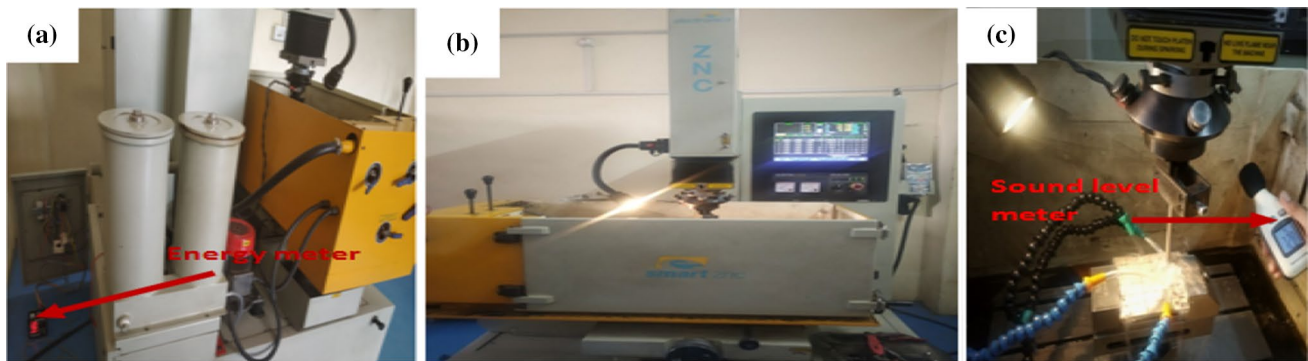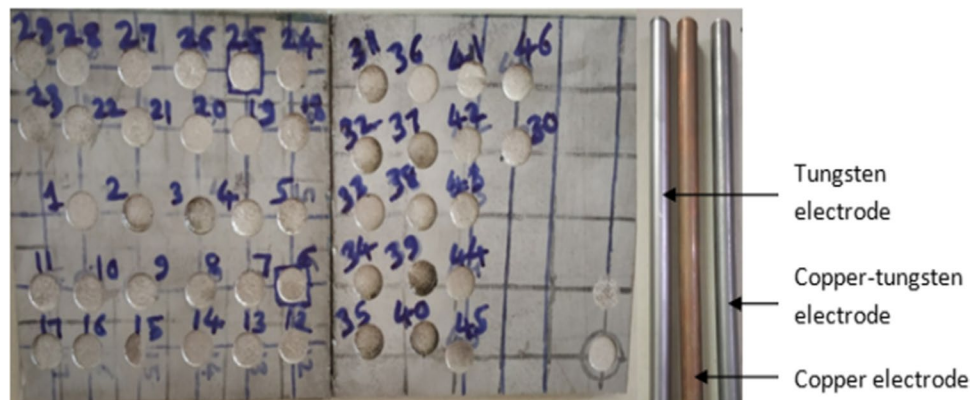**Fig. 2** Die-sinking ZNC EDM machine experimental set-up (**b**) with energy meter (**a**) and sound level meter (**c**)

Fig. 3 Nimonic C263 workpiece with the three electrodes

Tungsten electrode

Copper-tungsten electrode

Copper electrode

operation. Machining noise values are recorded five times for each experimental run. Finally, the average of the obtained values is calculated to get the final reading for each experiment.

3.2.3 Calculation of MRR and EWR

To calculate the MRR and TWR, a precise weighing machine (accuracy 0.01 g) is used to measure the weight loss of workpiece and electrodes before and after machining. The workpiece and electrode weight loss are used to calculate MRR and TWR using Eqs. 11 and 12. The EWR is calculated by using Eq. 13.

$$\text{MRR} = \frac{1000 \times \Delta W_w}{\rho_w \times T} \tag{11}$$

$$\text{TWR} = \frac{1000 \times \Delta W_t}{\rho_t \times T} \tag{12}$$

$$\text{EWR} = \frac{100 \times \text{TWR}}{\text{MRR}} \tag{13}$$

where ΔW_w is the loss of weight due to machining of the workpiece in gram (g), ρ_w is the density of the workpiece ($\rho_w = 8360$ kg/m^3) and T is the time of machining. TWR represents the tool wear rate in mm^3/min, ΔW_t is the weight loss due to machining of the tool in gram (g), ρ_t is the density of tool material ($\rho_{copper} = 8960$ kg/m^3, $\rho_{tungsten} = 19,600$ kg/m^3 and $\rho_{copper–tungsten} = 15,000$ kg/m^3).

3.2.4 Calculation of Surface Roughness (R_a)

For measuring the surface roughness of the machined surface, a surface roughness tester Mitutoyo Surftest SJ-210 is used. The roughness measurement is conducted five times on the machined surface of the workpiece. After recording the roughness values, the average of the five readings is taken as the final measurement.

3.2.5 Calculation of Radial Overcut (*C*)

The difference between the diameter of cavity produced on the workpiece and electrode diameter is called radial overcut. The radial overcut should be less for precise machining. Radial overcut is calculated by using the following relation.

$$\text{Radial overcut} \,(C) = \frac{d_2 - d_1}{2} \tag{14}$$

Here, d_2 is the diameter of the hole produced after machining, and d_1 is the diameter of the electrode

The experiments are conducted as per RSM Box–Behnken design to evaluate the effect of identified input process parameters on the responses, viz. SEC, machining noise (*N*), MRR, EWR, surface roughness (R_a), radial over cut (*C*) etc. Forty-six experiential runs are conducted to extract the information from the study. Table 5 shows the experimental design matrix along with obtained performance measures and calculated values of the net outranking flow obtained after application of PROMITHEE approach. The highest value of net outranking flow is obtained at run order; number 7 is highlighted in bold font.

3.3 Results and Discussions

The experiments are conducted as per Box–Behnken design to explore the machinability of Nimonic C263 workpiece with three different electrodes, viz. Tungsten, copper–tungsten and copper etc. Analysis of variance (ANOVA) is conducted on the performance measures to study the influence of each individual process parameters on the responses. The ANOVA table is obtained for the responses after elimination of the insignificant parameters from the table at the significance level of 0.05. The *R*-squared (R^2) and adjacent *R*-squared (Adj-R^2) values are found to be quite large for the responses ranging over ninety percentages. It is also observed that lack of fit is not significant for all responses. The Cor Total in the ANOVA table represents the "corrected total sum of squares". The term "Cor total" is important for calculating the individual percentage contribution of each parameter on the responses. The percentage contribution of individual parameter is calculated by dividing individual sum of squares of each parameter with Cor total. Similar types of calculations are reported by previous researchers [14, 67, 68]. Table 6 shows the ANOVA table for SEC along with the percentage contribution of each parameter. ANOVA table of SEC shows T_{on} is the most influential parameter with a percentage contribution of 48.02% followed by electrode material, voltage, discharge current, and duty factor, respectively. Table 7 represents the ANOVA table for machining noise (*N*) along with the percentage contribution of each parameter. The table shows that discharge current is the most important parameter for noise with a percentage contribution of 40.93%. Duty factor is found to be insignificant factor for machining noise (*N*). Table 8 shows the ANOVA table for MRR along with the percentage contribution of each parameter. It shows that the highest significant factor for MRR is electrode material with 37.37% percentage contribution followed by discharge current with 16.42% contribution. Table 9 shows the ANOVA table for EWR along with the percentage contribution of each parameter. It shows the most dominant parameter for EWR is the electrode material with a 70.59% percentage contribution, and discharge current is the second-highest significant factor with a percentage contribution of 21.97%. Table 10 represents the

Table 5 Experimental design along with obtained performance measures and net outranking flow with rank

Run	A	B	C	D	E	SEC (Avg) (J/mm^3)	N (dB)	MRR (mm^3/min)	EWR (%)	Surface roughness (μm)	Radial overcut (C) (mm)	Net outranking flow (∅)	Rank
1	− 1	− 1	0	0	0	0.528630	80.5	3.405	1.714	11.19	0.032	20.681	4
2	1	− 1	0	0	0	0.784753	87.6	5.352	4.892	18.75	0.07	5.081	16
3	− 1	1	0	0	0	0.757667	82.4	3.326	1.977	10.89	0.031	13.615	11
4	1	1	0	0	0	1.609640	91.6	3.653	5.048	17.06	0.079	− 17.259	40
5	0	0	− 1	− 1	0	0.628931	82.7	2.862	3.326	13.91	0.036	1.026	20
6	0	0	− 1	− 1	0	2.003710	82.5	2.695	3.884	15.8	0.052	− 21.909	44
7	**0**	**0**	**− 1**	**1**	**0**	**0.353010**	**82.9**	**5.099**	**3.773**	**13.82**	**0.039**	**23.650**	**1**
8	0	0	− 1	1	0	1.516000	83.8	3.562	4.960	16.08	0.058	− 9.515	35
9	0	− 1	0	0	− 1	1.160540	78.5	2.585	7.349	12.98	0.023	− 4.214	27
10	0	1	0	0	− 1	1.830070	81.2	2.295	7.838	13.86	0.038	− 18.782	41
11	0	− 1	0	0	1	0.506671	85.5	5.921	0.540	16.52	0.058	18.911	7
12	0	1	0	0	1	1.131470	88.3	3.712	2.062	14.56	0.069	0.654	21
13	− 1	0	− 1	0	0	0.316252	81.4	3.415	1.537	11.44	0.028	22.471	2
14	1	0	− 1	0	0	0.481559	88.1	5.233	4.721	17.25	0.075	7.754	14
15	− 1	0	− 1	0	0	1.136050	82.5	2.852	2.045	11.94	0.032	2.442	19
16	1	0	− 1	0	0	1.974410	92.8	3.829	5.894	18.84	0.069	− 17.021	39
17	0	0	0	1	− 1	1.688560	78.8	2.132	7.449	12.05	0.021	− 19.369	42
18	0	0	0	1	− 1	1.264490	81.1	2.847	7.349	12.98	0.032	− 6.479	30
19	0	0	0	− 1	1	1.025350	87.6	3.511	0.903	15.95	0.054	− 1.825	24
20	0	0	0	1	1	0.616227	88.6	5.842	0.945	14.99	0.067	16.444	8
21	0	− 1	− 1	0	0	0.404095	80	3.712	3.418	15.65	0.038	16.339	10
22	0	1	− 1	0	0	0.443412	84.6	4.736	3.896	12.23	0.054	16.398	9
23	0	− 1	− 1	0	0	1.378250	83.5	3.265	3.968	15.76	0.042	− 11.251	37
24	0	1	− 1	0	0	2.516980	87.5	2.503	4.961	14.95	0.057	− 28.563	46
25	− 1	0	0	− 1	0	0.855784	82.1	2.524	1.420	11.66	0.025	4.816	18
26	1	0	0	− 1	0	1.193750	89.5	4.222	5.573	18.02	0.079	− 6.597	31
27	− 1	0	0	1	0	0.587276	80.7	3.678	1.695	11.86	0.035	22.415	3
28	1	0	0	0	0	1.023560	89.7	4.924	5.803	17.45	0.078	− 0.533	22
29	0	1	0	− 1	− 1	1.362750	79.8	3.082	7.619	12.88	0.033	− 1.491	23
30	0	0	− 1	0	− 1	2.629020	82	2.054	8.892	13.02	0.025	− 20.024	43
31	0	0	− 1	0	1	0.315679	85.2	5.702	0.602	14.98	0.066	20.041	5
32	0	0	− 1	0	1	1.394630	89.2	3.872	1.534	16.23	0.062	− 3.109	25
33	− 1	0	0	0	− 1	1.142250	76.6	1.891	4.911	9.05	0.015	− 4.294	28
34	1	0	0	0	− 1	1.511240	84.6	3.335	9.180	14.96	0.045	− 10.202	36
35	− 1	0	0	0	1	0.611552	85.7	3.532	0.519	12.56	0.038	13.014	12
36	1	0	0	0	1	0.875456	95.4	5.757	2.915	19.12	0.1	4.877	17
37	0	− 1	0	− 1	0	0.778816	83.5	3.852	3.591	15.65	0.042	12.019	13
38	0	1	0	− 1	0	1.683370	83.8	2.495	3.806	14.75	0.055	− 22.746	45
39	0	− 1	0	1	0	0.615511	79.7	4.874	3.659	15.17	0.041	19.779	6
40	0	1	0	1	0	1.084710	87	3.872	4.203	14.35	0.055	6.678	15
41	0	0	0	0	0	1.217860	83.4	2.956	3.742	14.65	0.045	− 6.645	32
42	0	0	0	0	0	1.074940	83.4	3.564	3.662	14.75	0.066	− 5.179	29
43	0	0	0	0	0	1.417730	82.5	2.631	3.081	14.59	0.049	− 3.224	26
44	0	0	0	0	0	1.011470	83.6	3.545	3.972	14.39	0.045	− 13.393	38
45	0	0	0	0	0	1.447830	83.1	2.685	3.737	14.05	0.049	− 8.217	33
46	0	0	0	0	0	1.143520	84.2	3.300	3.752	14.32	0.049	− 8.620	34

Table 6 ANOVA outcomes for SEC

Source	Sum of squares	df	Mean square	F value	p value Prob > F	Percentage contribution	
Model	12.87	10	1.29	56.43	< 0.0001		Significant
A	0.77	1	0.77	33.94	< 0.0001	5.64	
B	1.5	1	1.5	65.81	< 0.0001	10.98	
C	6.56	1	6.56	287.59	< 0.0001	48.02	
D	0.49	1	0.49	21.45	< 0.0001	3.59	
E	2.33	1	2.33	102.38	< 0.0001	17.06	
$A \times C$	0.11	1	0.11	4.97	0.0324	0.81	
$B \times C$	0.3	1	0.3	13.25	0.0009	2.20	
A^2	0.69	1	0.69	30.07	< 0.0001	5.05	
B^2	0.12	1	0.12	5.37	0.0264	0.88	
D^2	0.18	1	0.18	8.01	0.0076	1.32	
Residual	0.8	35	0.023				
Lack of fit	0.64	30	0.021	0.66	0.7869		Not significant
Pure error	0.16	5	0.032				
Cor total	13.66	45					

Table 7 ANOVA outcomes for machining noise (N)

Source	Sum of squares	df	Mean square	F value	p-value Prob > F	Percentage contribution	
Model	661.17	7	94.45	110.57	< 0.0001		Significant
A	283.92	1	283.92	332.38	< 0.0001	40.93	
B	47.61	1	47.61	55.73	< 0.0001	6.86	
C	22.8	1	22.8	26.69	< 0.0001	3.29	
D	0.56	1	0.56	0.66	0.4221	0.08	
E	247.28	1	247.28	289.47	< 0.0001	35.65	
$B \times D$	12.25	1	12.25	14.34	0.0005	1.77	
A^2	46.75	1	46.75	54.73	< 0.0001	6.74	
Residual	32.46	38	0.85				
Lack of fit	30.89	33	0.94	2.97	0.1127		Not significant
Pure error	1.57	5	0.31				
Cor total	693.63	45					

ANOVA for surface roughness. The table shows the highest influencing factor for surface roughness is the discharge current with a percentage contribution of 72.49% and followed by electrode material with a percentage contribution of 14.99%. Table 11 shows the ANOVA table for radial overcut along with the percentage contribution of each parameter. Table shows the most influencing parameter for radial overcut is discharge current having a percentage contribution of 53.73% followed by electrode material with a contribution of 33.13%. The duty factor is found to be insignificant parameters for EWR and radial overcut. Table 12 represents the ANOVA table for net outranking flow along with the percentage contribution of each parameter. It shows that pulse on time is the most dominating factor for net outranking flow with percentage contribution of 30.69% followed by electrode material, discharge current, and

voltage. Duty factor has a less effect on net outranking flow with a percentage contribution of 6.99%.

3.4 Parametric Study on the Responses

3.4.1 Parametric Study on Specific Energy Consumption (SEC)

While machining hard and low conductive materials, the EDM power supply consumes a lot of electrical energy, thus increasing cost of manufacturing of each product. Therefore, to enhance productivity energy efficient machining operation is vital. To meet the above requirement SEC is considered as an important performance measure in this work. The surface plots for SEC with various process parameters are obtained using

Table 8 ANOVA outcomes for MRR

Source	Sum of squares	df	Mean square	F value	p-value Prob > F	Percentage contribution	
Model	46.42	10	4.64	29.3	< 0.0001		Significant
A	8.53	1	8.53	53.84	< 0.0001	16.42	
B	2.54	1	2.54	16.03	0.0003	4.89	
C	5.3	1	5.3	33.46	< 0.0001	10.20	
D	6.77	1	6.77	42.71	< 0.0001	13.03	
E	19.42	1	19.42	122.59	< 0.0001	37.37	
$A \times B$	0.66	1	0.66	4.14	0.0495	1.27	
$B \times C$	0.8	1	0.8	5.03	0.0313	1.54	
$B \times E$	0.92	1	0.92	5.81	0.0213	1.77	
$D \times E$	0.65	1	0.65	4.12	0.05	1.25	
A^2	0.83	1	0.83	5.26	0.028	1.60	
Residual	5.54	35	0.16				
Lack of fit	4.68	30	0.16	0.9	0.6236		Not significant
Pure error	0.87	5	0.17				
Cor total	51.96	45					

Table 9 ANOVA outcomes for EWR

Source	Sum of squares	df	Mean square	F value	p-value Prob > F	Percentage contribution	
Model	221.1	8	27.64	193.03	< 0.0001		Significant
A	49.73	1	49.73	347.34	< 0.0001	21.97	
B	1.36	1	1.36	9.48	0.0039	0.60	
C	3.28	1	3.28	22.92	< 0.0001	1.45	
D	0.37	1	0.37	2.59	0.1162	0.16	
E	159.81	1	159.81	1116.22	< 0.0001	70.59	
$A \times E$	0.88	1	0.88	6.13	0.018	0.39	
C^2	0.71	1	0.71	4.97	0.0319	0.31	
E^2	5.42	1	5.42	37.85	< 0.0001	2.39	
Residual	5.3	37	0.14				
Lack of fit	4.84	32	0.15	1.67	0.2994		Not significant
Pure error	0.45	5	0.091				
Cor total	226.4	45					

Design-Expert-11 software. The response surface plot for discharge current and pulse-on-time is shown in Fig. 4a. The figure shows that SEC increases with increase in discharge current and pulse-on-time. This is obvious, as both the parameters significantly dominate the spark energy, can cause significant rise of SEC. Figure 4b shows the response surface plot for SEC with electrode material and discharge current. The figure shows that SEC is maximum while machining with Tungsten electrode and is minimum with copper electrode while machining on Nimonic C263 workpiece. The copper–tungsten consumes SEC value those between copper and tungsten electrode. The copper electrode exhibits the highest MRR, so the energy consumption is less in a copper electrode. More energy is required to detach the material from a workpiece in the form of debris when the MRR is high. The input energy is utilized to remove the material, and because of this, we can say that energy utilization efficiency is strong in the copper electrode compared to tungsten and copper–tungsten electrodes.

The tungsten electrode produces low MRR as against copper and copper–tungsten electrode. The energy consumption is higher in the tungsten electrode because the workpiece utilizes less input energy and more energy goes into the environment. A similar finding is also observed in the study reported by Zhang et al. [3]. Figure 4c shows the response surface plot for SEC with discharge current and voltage. The figure shows that SEC increases with increase in discharge current and voltage. As discharge current increases, more energy is utilized for removing

Table 10 ANOVA outcomes for Surface roughness (R_a)

Source	Sum of squares	df	Mean square	F value	p-value Prob > F	Percentage contribution	
Model	214.75	9	23.86	104.05	< 0.0001		Significant
A	161.67	1	161.67	704.97	< 0.0001	72.49	
B	5.09	1	5.09	22.17	< 0.0001	2.28	
C	6.84	1	6.84	29.82	< 0.0001	3.07	
D	0.074	1	0.074	0.32	0.5729	0.03	
E	33.44	1	33.44	145.8	< 0.0001	14.99	
$B \times C$	1.7	1	1.7	7.43	0.0099	0.76	
$B \times E$	2.02	1	2.02	8.79	0.0053	0.91	
$D \times E$	0.89	1	0.89	3.89	0.0562	0.40	
E^2	3.03	1	3.03	13.23	0.0009	1.36	
Residual	8.26	36	0.23				
Lack of fit	7.93	31	0.26	3.88	0.0675		Not significant
Pure error	0.33	5	0.066				
Cor total	223.01	45					

Table 11 ANOVA outcomes for Radial overcut (C)

Source	Sum of squares	df	Mean square	F value	p-value Prob > F	Percentage contribution	
Model	0.014	5	0.00274	69.74	< 0.0001		Significant
A	0.00806	1	0.00806	204.91	< 0.0001	53.73	
B	0.00053	1	0.00053	13.46	0.0007	3.53	
C	0.00005	1	0.00005	1.25	0.2709	0.33	
D	0.00011	1	0.00011	2.67	0.1099	0.70	
E	0.00497	1	0.00497	126.43	< 0.0001	33.13	
Residual	0.00157	40	0.00004				
Lack of fit	0.00127	35	0.00004	0.59	0.8399		Not significant
Pure error	0.00031	5	0.00006				
Cor total	0.015	45					

Table 12 ANOVA outcomes for Net outranking flow

| Source	Sum of squares	df	Mean square	F value	p value	Percentage contribution	
Model	7895.57	11	717.78	21.59	< 0.0001		Significant
A	1041.01	1	1041.01	31.31	< 0.0001	11.53	
B	931.71	1	931.71	28.03	< 0.0001	10.32	
C	2770.29	1	2770.29	83.33	< 0.0001	30.69	
D	630.94	1	630.94	18.98	0.0001	6.99	
E	1143.77	1	1143.77	34.41	< 0.0001	12.67	
$D \times E$	318.75	1	318.75	9.59	0.0039	3.53	
A^2	533.31	1	533.31	16.04	0.0003	5.91	
B^2	277.4	1	277.4	8.34	0.0067	3.07	
D^2	247.9	1	247.9	7.46	0.0099	2.75	
Residual	1130.28	34	33.24				
Lack of fit	986.32	28	35.23	1.47	0.3339		Not significant
Pure error	143.96	6	23.99				
Cor total	9025.85	45					
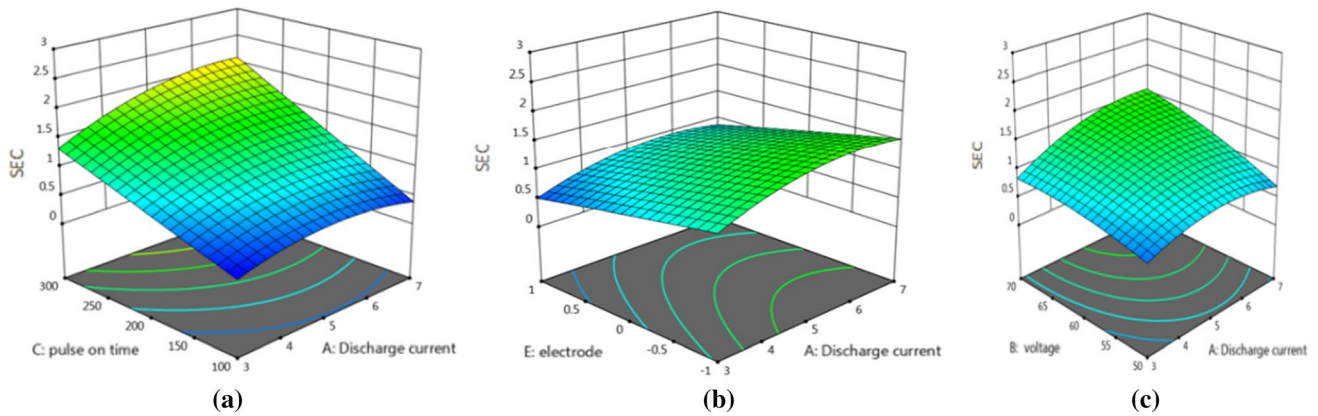
Fig. 4 **a** Response surface plots of SEC vs discharge current and pulse on time (μs), **b** SEC versus discharge current and electrode material, **c** SEC versus discharge current and voltage

material, and it increases energy consumption. The current and voltage have a low influence on the SEC.

3.4.2 Parametric Study on Machining Noise (*N*)

Machining noise is an important performance measure as it has a serious effect on the industrial environment. It can severely affect the concentration of the tool engineers by creating undesirable sounds in the workshop. Therefore, to achieve productivity, it should be as low as possible during machining. Figure 5a shows the variation of machining noise (*N*) with discharge current for the different electrode materials. The figure shows that machining noise (*N*) increases with increase in discharge current and it attains the highest value while machining with copper electrode. Increase in discharge current increases the spark energy across the electrodes, thus increasing MRR and EWR. This phenomenon causes creation of unwanted and undesirable sound during machining and in turn causes spike in the machining

noise (*N*). The copper electrode produces highest machining noise in comparisons with the copper–tungsten and tungsten electrode. Tungsten electrode produces the least magnitude noise during machining due to smaller MRR. Copper–tungsten electrode produces machining noise value those in between copper and tungsten. Figure 5b shows the surface plot for machining noise (*N*) with pulse-on-time and discharge current. Increase in pulse-on-time directly increases the spark energy creating abnormal discharges in between electrodes and thus increasing the machining noise (*N*). A similar observation is also reported by previous researchers [3]. Moreover, with the increase in voltage, the machining noise increases slowly, owing to increase in spark energy and discharges. However, voltage has a little effect on machining noise as observed in Fig. 5c.
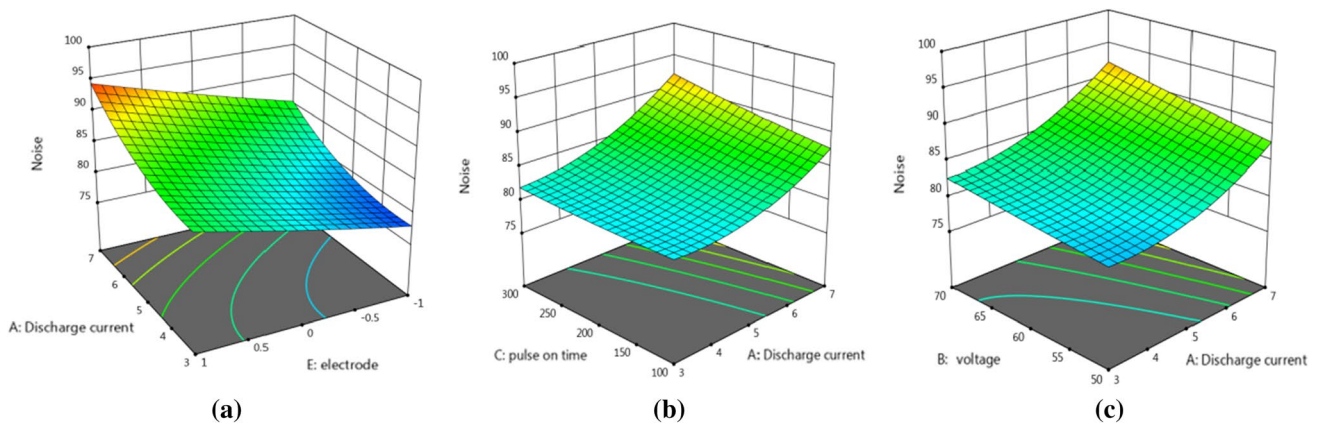
Fig. 5 **a** Response surface plots of machining noise versus electrode and discharge current, **b** machining noise versus pulse on time (μs) and discharge current, **c** machining noise versus voltage and discharge current

3.4.3 Parametric Study on MRR

MRR is the most important performance measures of EDM as it directly influences the machining performance and productivity of the process. Figure 6a shows the surface plot of MRR with discharge current and voltage. From the figure, it can be seen that MRR decreases with increase in voltage. When voltage increases unfavourable concentrated discharge occurs due to inadequate cooling of work material, which in turn reduces MRR. The figure also shows that MRR increases briskly, with increase in discharge current. Increase in discharge current significantly increases the spark energy, which in turn causes vaporization and melting of material from workpiece and thus increasing MRR. Figure 6b shows the variation of MRR with electrode material and discharge current. It shows that MRR shows an increasing trend with increase in discharge current for all three electrodes while machining Nimonic C263 workpiece. The figure also shows tungsten electrode produces least MRR in comparison with other two electrodes. The copper electrode produces highest material removal efficiency owing to higher value of thermal conductivity than the tungsten and copper–tungsten electrode. Copper–tungsten electrode produces MRR value those in between copper and tungsten electrode.

Similarly, Fig. 6c surface plot of MRR variation with discharge current and pulse on time represents that MRR will decrease along with the pulse on time. When there is an increase in pulse on time, the plasma channel's pressure decreases due to the continuous application of the same heat flux for a longer duration. As the molten metal's volume remains unaffected, a further increase in pulse-on-time results in a decrease of MRR [14]. Similarly, from the response surface plot of MRR with discharge current and duty factor, it is observed that MRR increases with increase in discharge current and duty factor. Increasing duty factor means increasing the number of sparks per unit time, which in turn removes more material from the work surface and thus increasing in MRR.

3.4.4 Parametric Study on EWR

The EWR is another important performance measure as it can directly influence the machining cost and time in the industry. For better machining performance, the electrode wear should be as less as possible in a machining operation. Figure 7a shows the response surface plot of EWR variation with discharge current and electrode. It shows that EWR shows an increasing trend with an increase in discharge current for all three electrodes while machining Nimonic C263 workpiece. This is because an increase in discharge current increases spark energy and hence more heat is generated across the electrodes, which causes the melting of the electrodes. The surface plot shows the EWR is less for the copper electrode and high for the tungsten electrode while machining Nimonic C263. EWR values for copper–tungsten electrode showed in the middle of copper and tungsten. The copper electrode shows less erosion due to its high thermal conductivity. The heat transfer occurs quickly in the body of copper electrode as it has high thermal conductivity resulting in less EWR. As copper and copper–tungsten electrodes have good thermal conductivity than the tungsten electrode, the erosion of tungsten electrode is faster in comparison with other electrodes. Figure 7b shows the variation of EWR with pulse on time and discharge current. From figure, it can be seen that EWR increases with pulse on time. As pulse on time increases, machining rate will increase, resulting in high EWR. Figure 7c shows the EWR variation with voltage and discharge current. The figure shows the EWR increases slowly with increasing voltage. Similarly, from the response surface plot of EWR with discharge current and duty factor, it is observed that EWR increases slowly with the duty factor. At high values of duty factor, the spark holds itself for a longer time resulting in increase in EWR. The voltage and duty factor do not contribute more to the variation of EWR.
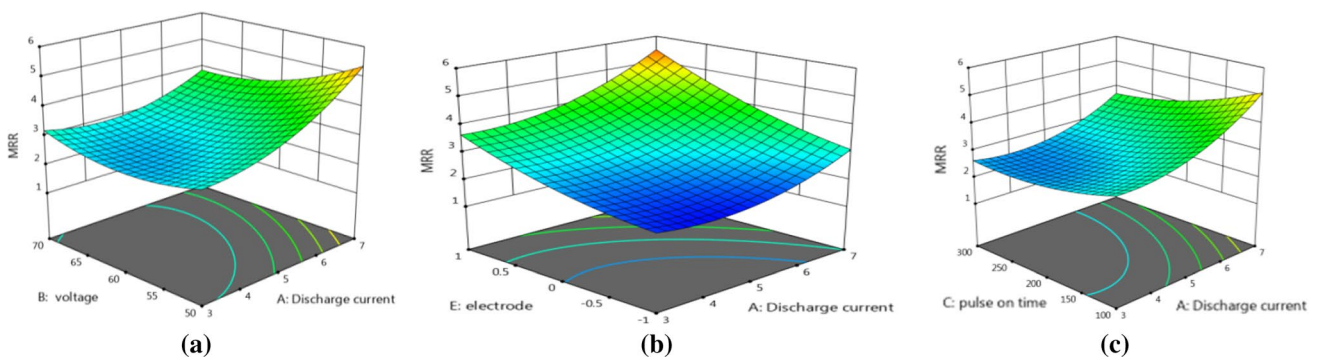
Fig. 6 **a** Response surface plots of MRR vs discharge current and voltage, **b** MRR vs discharge current and electrode and **c** MRR vs discharge current and pulse on time
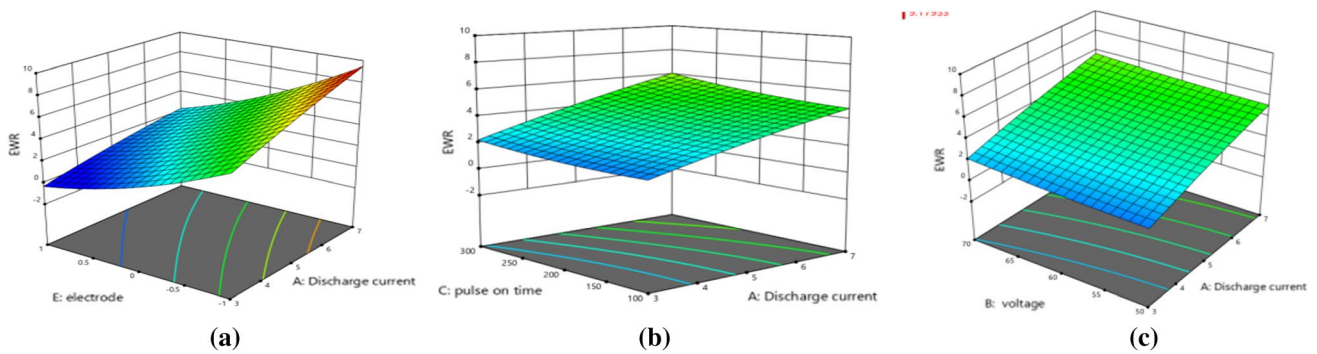
Fig. 7 **a** Response surface plots of EWR versus discharge current and electrode, **b** EWR versus discharge current and pulse-on-time **c** EWR versus discharge current and voltage

3.4.5 Parametric Study on Surface Roughness (R_a)

The EDM machined surface consists of numerous microcracks, voids and debris due to occurrence of continuous spark discharges on the workpieces after machining. However, aerospace and automotive components require high-quality finished parts with accurately defined features. In this concern, the machined surface quality is an important performance measure for EDM process. Figure 8a shows the surface plot of surface roughness with electrode material and discharge current. From the figure it can be seen that copper electrode exhibits the poor performance with regard to surface quality of the machined surface owing to higher MRR compared to copper–tungsten and the tungsten electrode. Tungsten electrode produces finest machined surfaced quality due to smaller material removal efficiency. The copper–tungsten electrode produces machined surface quality value those between the tungsten and copper electrodes while machining Nimonic C263 alloy. Likewise, Fig. 8b describes the influence of voltage and discharge current on surface roughness. It appears that the quality of the machined surface decays heavily with increase in the value

of discharge current for all three electrodes. Spark intensity increases with increase in the value of discharge current. This phenomenon causes larger dimension material removed from the work surface, which in turn reduces the machined surface quality. The figure also indicates that surface quality improves gradually with increase in value of voltage. This is because of the reduction in material remove rate which causes decrease in the value of surface roughness. A similar trend is also observed in the studies reported by Lee et al. [12]. Similarly, variation of surface roughness with the pulse on time and discharge current is shown in Fig. 8c. The figure shows that surface roughness increases with increase in the value of pulse-on-time. The spark energy increases due to increase in pulse-on-time, which causes larger size material to be eroded from work surface thus degrading the surface quality of the machined surface.

3.4.6 Parametric Study on Radial Overcut (*C*)

In EDM process, the accuracy of the drilled hole is evaluated in terms of radial overcut (*C*). To produce close
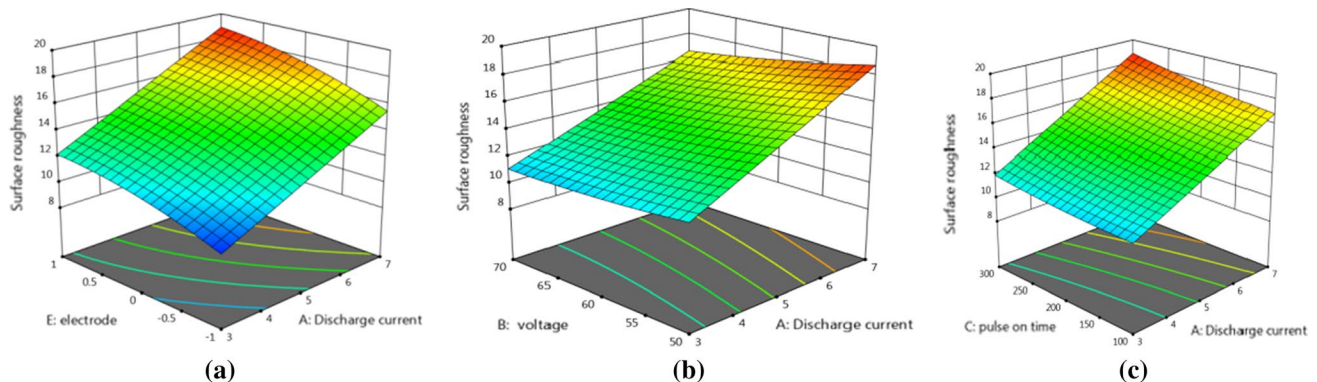
Fig. 8 **a** Response surface plots of surface roughness versus discharge current and electrode material, **b** surface roughness versus discharge current and voltage, **c** surface roughness versus discharge current and pulse on time (μs)
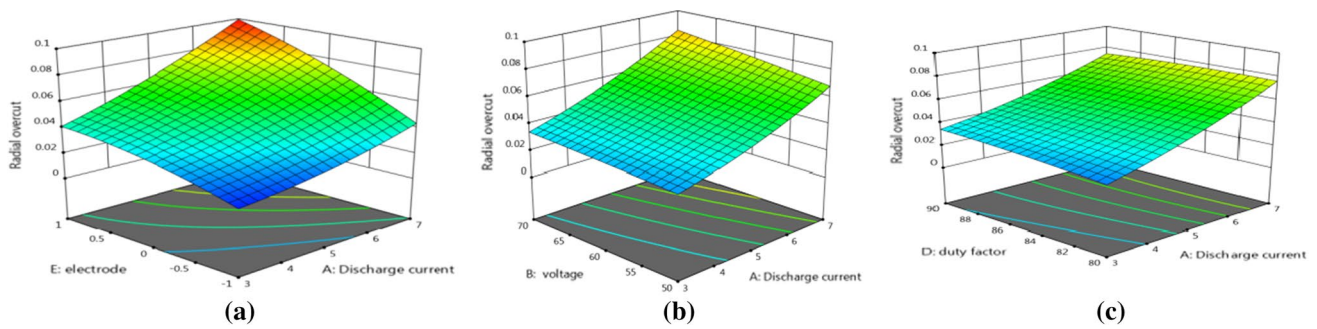
Fig. 9 **a** Response surface plots of radial overcut versus discharge current and electrode, **b** radial overcut versus discharge current and voltage and **c** radial overcut versus discharge current and duty factor

dimensionally accurate and precise EDMed parts, minimization of radial overcut is vital. Figure 9a shows the variation of radial overcut with discharge current and three electrodes. The figure shows that radial overcut increases with increase in the value of discharge current. As discharge current increases, the spark energy also increases, causing greater amount of material to be detached from the workpiece. This phenomenon produces wider and larger craters on the machined surface, resulting in production of larger overcut. The figure also shows that copper electrodes produce the wider radial over cut on the machined surface due to higher value of MRR. Tungsten produces the accurate and precise drilled holes while machining Nimonic C263 workpiece among the three electrodes. Copper–tungsten produces the overcut value those between copper and tungsten electrodes. Variation of radial overcut with voltage and discharge current is shown in Fig. 9b. It shows that radial overcut increases with increase in the value of discharge current and voltage due to increase in spark energy. Figure 9c shows the variation of radial overcut with duty factor and discharge current. From the figure, it can be seen that increasing duty factor increases the radial overcut gradually, due to increase in MRR. Similarly, from the surface plot of overcut with discharge current and pulse-on-time indicates that overcut increases with increase in a pulse-on-time. As pulse-on-time increases, spark energy also increases causing increase in overcut.

3.5 Scanning Electron Microscope (SEM) Analysis

A scanning electron microscope (SEM) Leica stereo scan 440 is used to conduct the microstructural investigation and to analyse the pre-machining and post-machining conditions of the workpiece obtained through various electrodes. Figure 10a shows the micrograph of the workpiece before machining. The machined surface before machining looks absolutely spotless and clean with no presence of melted

debris, globules, micro-cracks and melted drops. On the other hand, Fig. 10b–d shows the post-machining micrographs of the machined surface machined through copper, copper–tungsten and tungsten electrode, respectively, at the identical parametric conditions. It can be seen from the micrographs that the machined surface quality obtained with copper electrodes is the worst with the presence of plenty of micro-cracks, pores, melted material deposition due to higher material removal and improper flushing. The machined surface quality obtained from the tungsten is the finest with a lesser amount of melting, deposition, and minimal micro-cracks and pores compared to the other two electrodes. Owing to higher thermal conductivity the spark energy in between the copper electrode and Nimonic C263 workpiece is higher. This in turn increases the MRR but produces numerous adverse effect of on the machined surface like increasing micro-cracks and voids and recast layer. Instead, the spark energy is smaller in between the tungsten electrode and workpiece during machining due to smaller thermal conductivity of the tool, which produces finest machined surface with presence of least amount of micro-cracks and debris. Copper–tungsten electrode produces moderate quality machined surface those resulted in between copper and copper–tungsten electrode.

In this work, PROMETHEE method has been used to convert multiple responses into single equivalent response by calculating net outranking flow (Ø). Net outranking flow is used to rank the alternatives form best to the worst. From Table 5 it can be seen that experiment no. 7 is the best among the forty-six net outranking flow values obtained due to highest value of net outranking flow (Ø). The best result obtained through the PROMITHEE approach may further be improved by application of nature inspired computational technique like cuckoo search (CS) algorithm. To develop a hybrid optimization model in between PROMITHEE and cuckoo search (CS) algorithm, a mathematical model is developed by conducting regression analysis to relate the

(a)

(b)

(c)

(d)
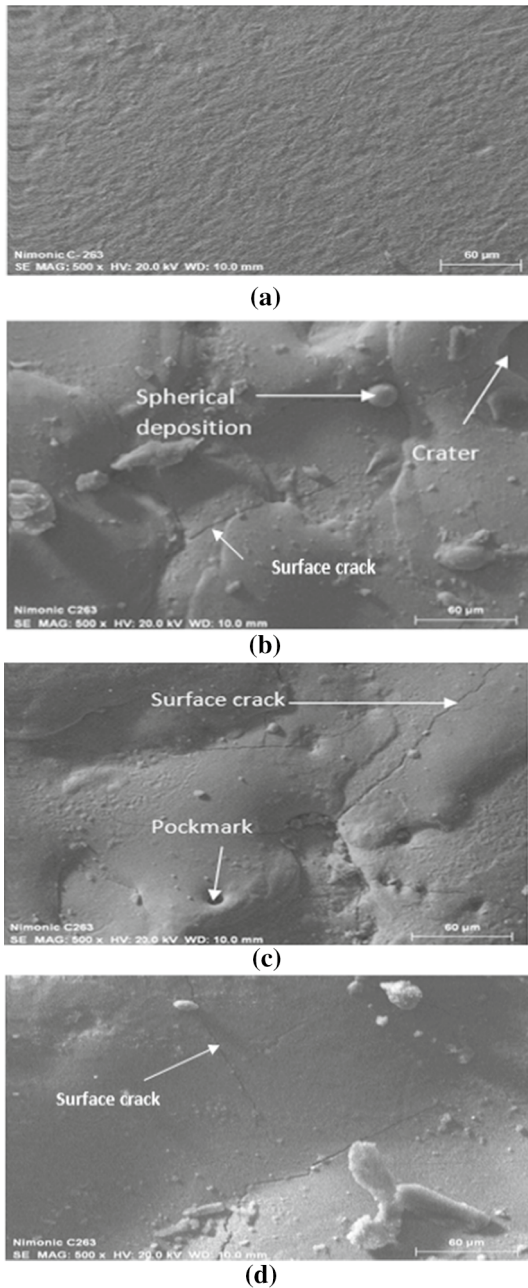
Fig. 10 SEM micrographs of Nimonic C-263 workpiece **a** before machining, **b** machined with copper, **c** machined with copper–tungsten, **d** machined with tungsten electrode at the parametric setting $A = 7$, $B = 60$, $C = 200$, $D = 85$

process parameters with the net outranking flow which can be used as an objective function in cuckoo search CS algorithm. The detail about the algorithm and hybrid optimization framework is discussed in Sect. 5. The quadratic model obtained through regression analysis is given by Eq. 15.

$$\begin{aligned} \text{Net outranking flow} = & -8.17 - 8.07A - 7.49B - 13.68C \\ & + 6.14D + 8.61E - 3.82AB - 1.19AC \\ & - 2.88AD - 0.5573AE - 4.34BC \\ & + 3.55BD - 2.79BE - 2.56CD - 0.2025CE \\ & + 8.52DE + 7.86A^2 + 5.66B^2 \\ & + 2.84C^2 + 5.26D^2 + 2.77E^2 \end{aligned} \tag{15}$$

4 Hybrid Optimization Strategy

4.1 The Cuckoo Search Algorithm

In this work, a hybrid optimization framework is proposed in attempting to develop a PROMITHEE-based cuckoo search (CS) algorithm to achieve the optimum machining condition. In the year 2009, Yang and Deb proposed a meta-heuristic computational technique, popularly known as cuckoo search optimization (CSO) algorithm [69]. The algorithm is simple, involves less computational techniques and rapidly converges to achieve the optimum solution [50, 70, 71]. The technique successfully applied to solve many engineering problems, viz. milling operation, travelling salesman, structural optimization etc. [51–53]. The natural behaviours of cuckoo bird are the stimulus of the algorithm, specifically, the obligate brood parasitism of cuckoo species by laying their eggs in another bird's nest. When the host bird finds cuckoo eggs in her nest, it depends either the host bird will throw that egg out or will leave it in the nest and start her own family at some other place. Bird nest having each egg specifies a possible solution, whereas a cuckoo's egg confirms a new better solution.

The algorithm depends up on three conditions which implements the similar behaviour of cuckoos in a system. The conditions are given in the following lines.

(a) Each cuckoo lays a single egg at a time and flings its egg in a random nest.
(b) The nest having the best quality of eggs will be passed on to next creation.
(c) The amount of hosts available is same, and the probability of an egg discovered by the host which is laid by a cuckoo is Pa $\in$ (0,1)

Yang and Deb proposed that the random-walk search style is performed better by Levy flights than simple random walk. A better answer is $X(t + 1)$ created using a Levy flight for cuckoo bird i by using following equation [69]:

$$X(i(t + 1)) = X(i(t)) + \propto \oplus \text{Levy}(\lambda) \tag{16}$$

where $\propto$ is the step size, $\oplus$ represents the entry-wise multi-plication operation, and λ is a Levy fight parameter.

Levy fight is a kind of random walk with the step length based on Levy distribution. It is introduced to the CS algorithm to get a Levy-fight-style intermittent scale-free search pattern. In [72], it was revealed that Levy fights are capable to maximize the efficiency of resource searches in the uncertain environment. The Levy distribution is defined as

$$L(s, \gamma, \mu) = \begin{cases} \sqrt{\frac{\gamma}{2\pi}} \exp\left[-\frac{\gamma}{2(s-\mu)}\right] \frac{1}{(s-\mu)^{3}/2} & 0 < \mu < s < 0 \\ 0 & \text{Otherwise} \end{cases} \tag{17}$$

where, $\mu > 0$ a minimum is step and γ is a scale parameter. The step length s can be calculated by Eq. 18.
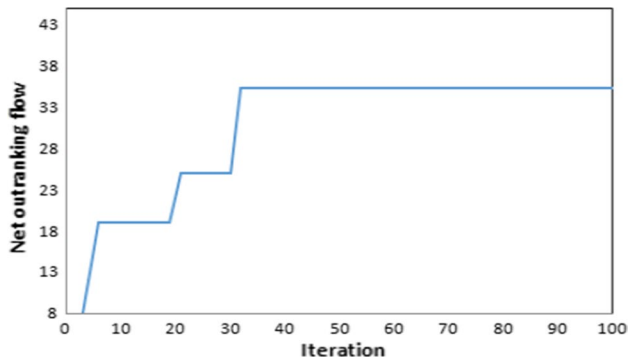
$$s = \frac{u}{|v|^{1/\beta}} \tag{18}$$

Here, β is an index, ranging between $1 \leq \beta \leq 2$. Where u and v are drawn from normal distribution

$$u \sim N(0, \sigma_u^2)$$
$$v \sim N(0, \sigma_v^2)$$

where N is normal distribution, σ_u and σ_v are as follows and can be obtained from Eq. 19

Fig. 11 Cuckoo search algorithm flowchart [71]
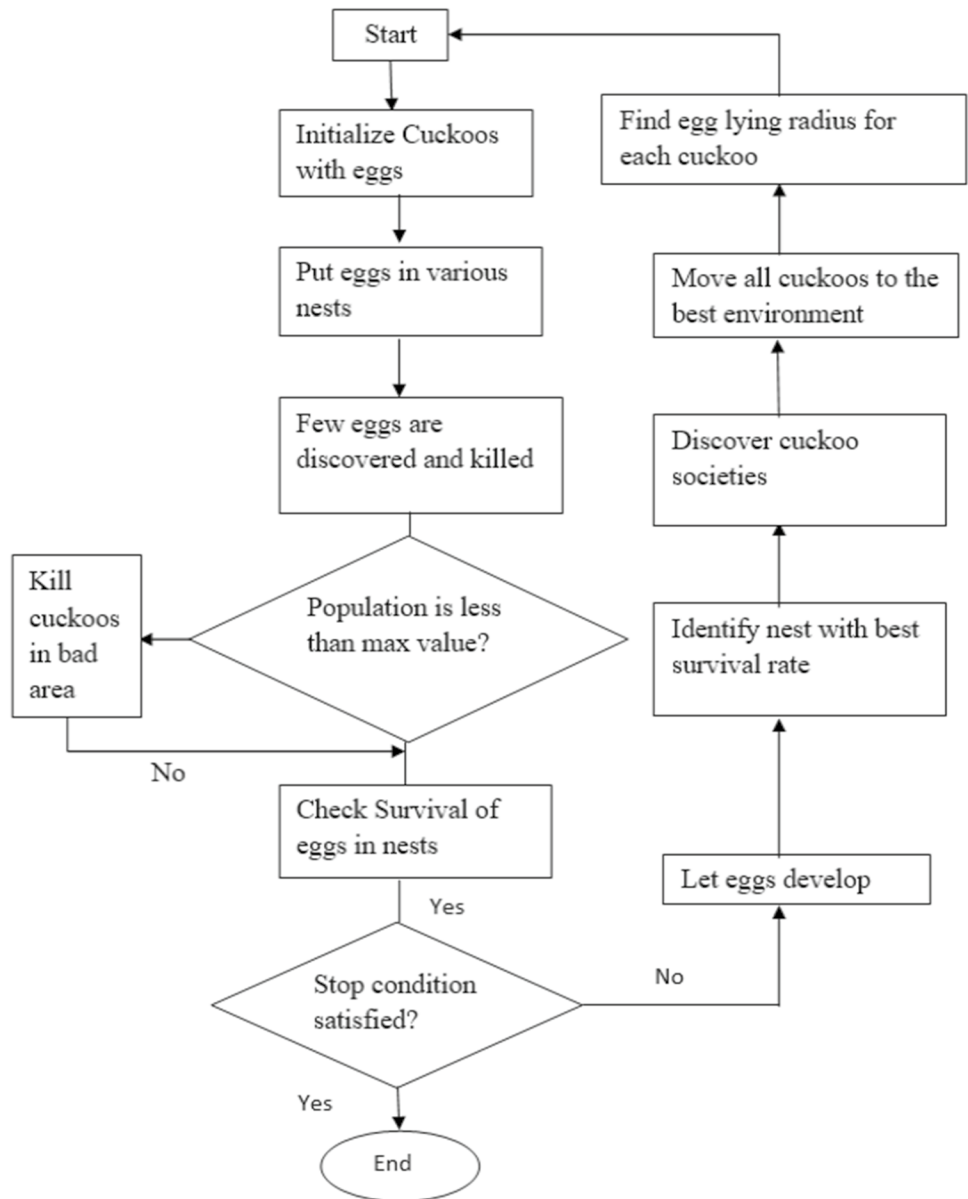
Fig. 12 Convergence plot for PROMITHEE-based cuckoo search algorithm

$$\sigma_u = \left\{ \frac{\Gamma(1 + \beta) \sin(\pi \beta / 2)}{\Gamma\left[(1 + \beta)/2\right] \beta 2^{(1 + \beta)/2}} \right\}^{1/\beta}, \quad \sigma_v = 1 \qquad (19)$$

where Γ is the gamma function and is given by

$$\Gamma(z) = \int_0^{\infty} t^{z-1} e^{-t} dt \qquad (20)$$

where z is a positive integer.

The algorithm is well explained with the help of following flow chart shown in Fig. 11.

4.2 PROMITHEE-Based Cuckoo Search (CS) Algorithm

The net outranking flow (Ø) values obtained through PRO-MITHEE approach are related with the process parameters by conducting a nonlinear regression analysis is given by Eq. 15. Furthermore, yet again an attempt is made to enhance the value of net outranking flow (Ø) by developing a hybrid optimization model (PROMITHEE-based cuckoo search algorithm). Electrode material is a qualitative parameter while voltage, discharge current, pulse-on-time and duty factor are quantitative process parameters. The quantitative parameters are real numbers that lie in the range [− 1, 1]. For the qualitative parameters, the nearest integer part of the real numbers is considered. The ranges of the qualitative parameters (electrode material) are considered in the manner if the values generated in between − 1 and 0.29, it is considered as − 1 or tungsten tool, if in between − 0.3 and 0.59 it is considered as 0 or copper–tungsten tool and if in between 0.6 and 1 considered as 1 or copper tool. Accordingly, Eq. 15 is used as an objective function in cuckoo search (CS) algorithm coded in MATLAB. The optimization problem was run in a core i5 processor on a Lenovo laptop to evaluate the potential of cuckoo search algorithm. The

Table 13 Confirmative test results along with comparisons of responses obtained by PROMETHEE and PROMITHEE-based cuckoo search algorithm

Method	A (Amp)	B (V)	C (µs)	D (%)	E	SEC (J/mm³)	Machining noise (N) (Db)	MRR (mm³/min)	EWR (%)	Surface roughness (R_a) (µm)	Radial overcut (C) (mm)	Net out-ranking flow (Ø)	Overall improve-ment
PROMETHEE	5	60	100	90	Copper–tungsten	0.3530	82.9	5.099	3.773	13.82	0.0390	23.65	
PROMITHEE-based cuckoo search	3	60	100	85	Copper	0.3215	80.2	5.556	3.529	13.17	0.0375	35.23	
% improvement						8.92%	3.25%	8.96%	6.46%	4.70%	3.84%		6.02%

tuning parameters of the algorithm are set at nest size 80, the elitism probability 60, and the repetition 100. This led to convergence of the solution and generation of optimum solution as $A = 3$, $B = 60$, $C = 100$, $D = 85$ and $E = $ copper tool. It is observed that the net outranking flow (Ø) has shown a significant improvement, in predicting a value of 35.23 by the application of the hybrid approach (PROMITHEE-based cuckoo search) thrashing the previous best value obtained through PROMITHEE approach. The convergence plot for the same is shown in Fig. 12.

In order to test the feasibility of the result obtained by the hybrid optimization strategy (PROMITHEE-based cuckoo search), a confirmative test is conducted on the optimum machining condition to validate the proposed work. It is seen that there is an overall improvement of 6.02% with an individual improvement of 8.92% for SEC, 3.25% for machining noise (N), 8.96% for MRR, 6.46% for EWR, 4.70% for surface roughness and 3.84% for radial overcut, respectively, for each response validating the proposed work. The confirmative test results and percentage improvement values for each of the responses have been furnished in Table 13. Similar, type of percentage improvement calculation is reported elsewhere [47].

5 Conclusions

The current research work explores the machinability of Nimonic C263 workpiece to meet the requirement of sustainable EDM machining. A hybrid optimization strategy (PROMITHEE-based cuckoo search) is implemented to achieve the optimum machining condition. The optimum machining condition is found to be $A = 3$A, $B = 60$V, $C = 100$μs, $D = 85$% and $E = $Copper. A confirmative test is conducted on the optimum machining condition showing an overall improvement of 6.02% validating the proposed work. This work is useful to achieve ideal machining conditions, enhance productivity, and environment friendly pleasant work environment to fulfil the need of sustainable machining. The important findings of the work is summarized as follows:

1. For sustainable machining viewpoint, copper electrode is found to be the best, as it consumes minimum specific energy (SEC) and produces acceptable machining noise (N).

2. The copper electrode exhibits the best performance among the other two electrodes with an objective of lower specific energy consumption. Pulse on time is the most influential parameter for SEC while machining Nimonic C263 workpiece.

3. Discharge current and electrode material have a significant impact on machining noise (N) during EDM of Nimonic C263 workpiece. The machining noise is smaller when machining with tungsten electrode as compared to other two electrodes.

4. The electrode material and discharge current have a significant effect on the MRR of Nimonic C263 in EDM. The copper electrode at a high level of discharge current produces higher MRR during EDM of Nimonic C263.

5. The electrode material and discharge current are the most influencing factors for EWR. Copper electrode is found to be the best among other two with respect to EWR.

6. Discharge current is found to be the most dominant factor for surface roughness in EDM of Nimonic C263 superalloy. Tungsten electrode produces the superior machined surface quality amid the three electrodes.

7. A lower value of discharge current can produce an accurate and precise cut during EDM of Nimonic C263. Tungsten electrode can be used to produce precise and accurate EDMed parts.

References

1. Rajesha, S.; Sharma, A.K.; Kumar, P.: On electro discharge machining of Inconel 718 with hollow tool. J. Mater. Eng. Perform. **21**(6), 882–891 (2012)
2. Sabur, A.; Ali, M.Y.; Maleque, M.A.; Khan, A.A.: Investigation of material removal characteristics in EDM of nonconductive ZrO_2 ceramic. Procedia Eng. **56**, 696–701 (2013)
3. Zhang, Z.; Yu, H.; Zhang, Y.; Yang, K.; Li, W.; Chen, Z.; Zhang, G.: Analysis and optimization of process energy consumption and environmental impact in electrical discharge machining of titanium superalloys. J. Clean. Prod. **198**, 833–846 (2018)
4. Ming, W.; Zhang, Z.; Wang, S.; Zhang, Y.; Shen, F.; Zhang, G.: Comparative study of energy efficiency and environmental impact in magnetic field assisted and conventional electrical discharge machining. J. Clean. Prod. **214**, 12–28 (2019)
5. Li, W.; Kara, S.: Characterising energy efficiency of electrical discharge machining (EDM) processes. Procedia Cirp **29**, 263–268 (2015)
6. Bagaber, S.A.; Yusoff, A.R.: Multi-objective optimization of cutting parameters to minimize power consumption in dry turning of stainless steel 316. J. Clean. Prod. **157**, 30–46 (2017)
7. Zhang, G.; Li, W.; Zhang, Y.; Huang, Y.; Zhang, Z.; Chen, Z.: Analysis and reduction of process energy consumption and thermal deformation in a micro-structure wire electrode electric discharge machining thin-wall component. J. Clean. Prod. **244**, 118763 (2020)
8. Franco, A.; Rashed, C.A.A.; Romoli, L.: Analysis of energy consumption in micro-drilling processes. J. Clean. Prod. **137**, 1260–1269 (2016)
9. Dong, H.; Liu, Y.; Li, M.; Zhou, Y.; Liu, T.; Li, D.; Sun, Q.; Zhang, Y.; Ji, R.: Sustainable electrical discharge machining using water in oil nanoemulsion. J. Manuf. Process. **46**, 118–128 (2019)

10. Singh, N.K.; Singh, Y.; Sharma, A.; Singla, A.; Negi, P.: An environmental-friendly electrical discharge machining using different sustainable techniques: a review. Adv. Mater. Process. Technol. (2020). https://doi.org/10.1080/2374068X.2020.1785210

11. Torres, A.; Puertas, I.; Luis, C.J.: Modelling of surface finish, electrode wear and material removal rate in electrical discharge machining of hard-to-machine alloys. Precis. Eng. **40**, 33–45 (2015)

12. Lee, S.H.; Li, X.: Study of the surface integrity of the machined workpiece in the EDM of tungsten carbide. J. Mater. Process. Technol. **139**(1–3), 315–321 (2003)

13. Rahul, D.S.; Masanta, M.; Biswal, B.B.; Mahapatra, S.S.: Analysis on surface characteristics of electro-discharge machined Inconel 718. Int. J. Mater. Prod. Technol. **56**(1–2), 135–168 (2018)

14. Mohanty, C.P.; Mahapatra, S.S.; Singh, M.R.: An intelligent approach to optimize the EDM process parameters using utility concept and QPSO algorithm. Eng. Sci. Technol. Int. J. **20**(2), 552–562 (2017)

15. Tai, T.Y.; Lu, S.J.; Chen, Y.H.: Surface crack susceptibility of electrodischarge-machined steel surfaces. Int. J. Adv. Manuf. Technol. **57**(9–12), 983 (2011)

16. Bhaumik, M.; Maity, K.: Effect of electrode materials on different EDM aspects of titanium alloy. Silicon **11**(1), 187–196 (2019)

17. Mohanty, A.; Talla, G.; Gangopadhyay, S.: Experimental investigation and analysis of EDM characteristics of Inconel 825. Mater. Manuf. Process. **29**(5), 540–549 (2014)

18. Ming, W.; Jia, H.; Zhang, H.; Zhang, Z.; Liu, K.; Du, J.; Shen, F.; Zhang, G.: A comprehensive review of electric discharge machining of advanced ceramics. Ceram. Int. **46**, 21813–21838 (2020)

19. Kolli, M.; Kumar, A.: Effect of dielectric fluid with surfactant and graphite powder on electrical discharge machining of titanium alloy using Taguchi method. Eng. Sci. Technol. Int. J. **18**(4), 524–535 (2015)

20. Kumar, S.; Dhingra, A.K.; Kumar, S.: Parametric optimization of powder mixed electrical discharge machining for nickel-based superalloy Inconel-800 using response surface methodology. Mech. Adv. Mater. Mod. Process. **3**(1), 7 (2017)

21. Kumar, S.; Batra, U.: Surface modification of die steel materials by EDM method using tungsten powder-mixed dielectric. J. Manuf. Process. **14**(1), 35–40 (2012)

22. Abdudeen, A.; Abu Qudeiri, J.E.; Kareem, A.; Ahammed, T.; Ziout, A.: Recent advances and perceptive insights into powder-mixed dielectric fluid of EDM. Micromachines **11**(8), 754 (2020)

23. Kumar, S.; Batish, A.; Singh, R.; Bhattacharya, A.: Effect of cryogenically treated copper–tungsten electrode on tool wear rate during electro-discharge machining of Ti–5Al–2.5 Sn alloy. Wear **386**, 223–229 (2017)

24. Goyal, A.: Investigation of material removal rate and surface roughness during wire electrical discharge machining (WEDM) of Inconel 625 super alloy by cryogenic treated tool electrode. J. King Saud Univ. Sci. **29**(4), 528–535 (2017)

25. Mishra, D.K.; Datta, S.; Masanta, M.: Effects of tool electrode on EDM performance of Ti–6Al–4V. Silicon **10**(5), 2263–2277 (2018)

26. Datta, S.; Biswal, B.B.; Mahapatra, S.S.: Electrical discharge machining of Inconel 825 using cryogenically treated copper electrode: emphasis on surface integrity and metallurgical characteristics. J. Manuf. Process. **26**, 188–202 (2017)

27. Srivastava, V.; Pandey, P.M.: Study of ultrasonic assisted cryogenically cooled EDM process using sintered (Cu–TiC) tooltip. J. Manuf. Process. **15**(1), 158–166 (2013)

28. Arshad, R.; Mehmood, S.; Shah, M.; Imran, M.; Qayyum, F.: Effect of distilled water and kerosene as dielectrics on machining rate and surface morphology of Al-6061 during electric discharge machining. Adv. Sci. Technol. Res. J. **13**, 162–169 (2019)

29. Niamat, M.; Sarfraz, S.; Aziz, H.; Jahanzaib, M.; Shehab, E.; Ahmad, W.; Hussain, S.: Effect of different dielectrics on material removal rate, electrode wear rate and microstructures in EDM. Procedia Cirp **60**, 2–7 (2017)

30. Chen, S.L.; Yan, B.H.; Huang, F.Y.: Influence of kerosene and distilled water as dielectrics on the electric discharge machining characteristics of Ti–6A1–4V. J. Mater. Process. Technol. **87**(1–3), 107–111 (1999)

31. Bose, G.; Mahapatra, K.: Multi criteria decision making of machining parameters for Die Sinking EDM Process. Int. J. Ind. Eng. Comput. **6**(2), 241–252 (2015)

32. Dewangan, S.; Gangopadhyay, S.; Biswas, C.K.: Multi-response optimization of surface integrity characteristics of EDM process using grey-fuzzy logic-based hybrid approach. Eng. Sci. Technol. Int. J. **18**(3), 361–368 (2015)

33. Saravanan, M.; Thiyagarajan, C.; Somasundaram, S.: Parametric optimization of wirecut-electrical discharge machining through cuckoo search algorithm. Mater. Today Proc. **22**, 681–687 (2019)

34. Mohanty, C.P.; Mahapatra, S.S.; Singh, M.R.: A particle swarm approach for multi-objective optimization of electrical discharge machining process. J. Intell. Manuf. **27**(6), 1171–1190 (2016)

35. Mohanty, C.P.; Mahapatra, S.S.; Singh, M.R.: An experimental investigation of machinability of Inconel 718 in electrical discharge machining. Procedia Mater. Sci. **6**, 605–611 (2014)

36. Jung, J.H.; Kwon, W.T.: Optimization of EDM process for multiple performance characteristics using Taguchi method and Grey relational analysis. J. Mech. Sci. Technol. **24**(5), 1083–1090 (2010)

37. Majumder, A.; Das, P.K.; Majumder, A.; Debnath, M.: An approach to optimize the EDM process parameters using desirability-based multi-objective PSO. Prod. Manuf. Res. **2**(1), 228–240 (2014)

38. Mohan, B.; Rajadurai, A.; Satyanarayana, K.G.: Electric discharge machining of Al-SiC metal matrix composites using rotary tube electrode. J. Mater. Process. Technol. **153–154**, 978–985 (2004)

39. Sahu, S.N.; Nayak, N.C.: Multi-objective optimisation of EDM process using ANN integrated with NSGA-II algorithm. Int. J. Manuf. Technol. Manag. **32**(4–5), 381–395 (2018)

40. Mandal, A.; Dixit, A.R.; Chattopadhyaya, S.; Paramanik, A.; Hloch, S.; Królczyk, G.: Improvement of surface integrity of Nimonic C263 super alloy produced by WEDM through various post-processing techniques. Int. J. Adv. Manuf. Technol. **93**(1–4), 433–443 (2017)

41. Rao, M.S.; Venkaiah, N.: Parametric optimization in machining of Nimonic-263 alloy using RSM and particle swarm optimization. Procedia Mater. Sci. **10**, 70–79 (2015)

42. Shastri, R.K.; Mohanty, C.P.: Machinability investigation on Nimonic C263 alloy in electric discharge machine. Mater. Today Proc **26**, 529–533 (2020)

43. Jadhav, P.S.; Mohanty, C.P.; Hotta, T.K.; Gupta, M.: An optimal approach for improving the machinability of Nimonic C-263 superalloy during cryogenic assisted turning. J. Manuf. Process. **58**, 693–705 (2020)

44. Jadhav, P.S.; Mohanty, C.P.; Shirguppikar, S.S.: Cryogenic treatment of Nimonic alloy-hard turning: state-of-the-art, challenges and future directions. Mater. Today Proc. **18**, 4120–4132 (2019)

45. Vulević, T.; Dragović, N.: Multi-criteria decision analysis for subwatersheds ranking via the PROMETHEE method. Int. Soil Water Conserv. Res. **5**(1), 50–55 (2017)

46. Karande, P.; Chakraborty, S.: Application of PROMETHEE-GAIA method for non-traditional machining processes selection. Manag. Sci. Lett. **2**(6), 2049–2060 (2012)

47. Rao, R.V.; Rai, D.P.; Balic, J.: Multi-objective optimization of abrasive waterjet machining process using Jaya algorithm and PROMETHEE Method. J. Intell. Manuf. **30**(5), 2101–2127 (2019)

48. Brans, J.; Vincke, P.: A preference ranking organisation method: the PROMETHEE method for MCDM. Manag. Sci. **31**(6), 647656 (1985)

49. Venkata Rao, R.; Patel, B.K.: Decision making in the manufacturing environment using an improved PROMETHEE method. Int. J. Prod. Res. **48**(16), 4665–4682 (2010)

50. Rakhshani, H.; Rahati, A.: Intelligent multiple search strategy cuckoo algorithm for numerical and engineering optimization problems. Arab. J. Sci. Eng. **42**(2), 567–593 (2017)

51. Araghi, S.; Khosravi, A.; Creighton, D.: Intelligent cuckoo search optimized traffic signal controllers for multi-intersection network. Exp. Syst. Appl. **42**(9), 4422–4431 (2015)

52. Naumann, D.; Evans, B.; Walton, S.; Hassan, O.: A novel implementation of computational aerodynamic shape optimisation using Modified Cuckoo Search. Appl. Math. Model. **40**(7–8), 4543–4559 (2016)

53. Huang, J.; Gao, L.; Li, X.: An effective teaching-learning-based cuckoo search algorithm for parameter optimization problems in structure designing and machining processes. Appl. Soft Comput. **36**, 349–356 (2015)

54. Ezilarasan, C.; Velayudham, A.: Theoretical predictions and experimental validations on machining the Nimonic C263 super alloy. Simul. Model. Pract. Theory **40**, 192–207 (2014)

55. Ezilarasan, C.; Velayudham, A.: An experimental analysis and measurement of process performances in machining of Nimonic C-263 super alloy. Measurement **46**(1), 185–199 (2013)

56. Ozgedik, A.; Cogun, C.: An experimental investigation of tool wear in electric discharge machining. Int. J. Adv. Manuf. Technol. **27**(5–6), 488–500 (2006)

57. Prasanna, P.; Sashank, T.V.; Manikanta, B.; Aluri, P.: Optimizing the process parameters of electrical discharge machining on AA7075-SiC alloys. Mater. Today Proc. **4**(8), 8517–8527 (2017)

58. Mohan, B.; Rajadurai, A.; Satyanarayana, K.G.: Electric discharge machining of Al-SiC metal matrix composites using rotary tube electrode. J. Mater. Process. Technol. **153**, 978–985 (2004)

59. Pradhan, B.B.; Masanta, M.; Sarkar, B.R.; Bhattacharyya, B.: Investigation of electro-discharge micro-machining of titanium super alloy. Int. J. Adv. Manuf. Technol. **41**(11–12), 1094 (2009)

60. Yan, B.H.; Wang, C.C.: The machining characteristics of Al_2O_3/6061Al composite using rotary electro-discharge machining with a tube electrode. J. Mater. Process. Technol. **95**(1–3), 222–231 (1999)

61. Manikandan, N.; Raju, R.; Palanisamy, D.; Binoj, J.S.: Optimisation of spark erosion machining process parameters using hybrid grey relational analysis and artificial neural network model. Int. J. Mach. Mach. Mater. **22**(1), 1–23 (2020)

62. Singh, H.: Experimental study of distribution of energy during EDM process for utilization in thermal models. Int. J. Heat Mass Transf. **55**(19–20), 5053–5064 (2012)

63. Ming, W.; Zhang, Z.; Wang, S.; Huang, H.; Zhang, Y.; Zhang, Y.; Shen, D.: Investigating the energy distribution of workpiece and optimizing process parameters during the EDM of Al6061, Inconel 718, and SKD11. Int. J. Adv. Manuf. Technol. **92**(9–12), 4039–4056 (2017)

64. Ming, W.; Shen, F.; Zhang, G.; Liu, G.; Du, J.; Chen, Z.: Green machining: a framework for optimization of cutting parameters to minimize energy consumption and exhaust emissions during electrical discharge machining of Al 6061 and SKD 11. J. Clean. Prod. (2020). https://doi.org/10.1016/j.jclepro.2020.124889

65. Sivapirakasam, S.P.; Mathew, J.; Surianarayanan, M.: Multi-attribute decision making for green electrical discharge machining. Expert Syst. Appl. **38**(7), 8370–8374 (2011)

66. Yadav, S.K.: Optimization of Green Electro-Discharge Machining Using VIKOR. Doctoral dissertation (2013)

67. Benyounis, K.Y.; Olabi, A.G.; Hashmi, M.S.J.: Effect of laser welding parameters on the heat input and weld-bead profile. J. Mater. Process. Technol. **164**, 978–985 (2005)

68. Pandiarajan, S.; Kumaran, S.S.; Kumaraswamidhas, L.A.; Saravanan, R.: Interfacial microstructure and optimization of friction welding by Taguchi and ANOVA method on SA 213 tube to SA 387 tube plate without backing block using an external tool. J. Alloys Compd. **654**, 534–545 (2016)

69. Yang, X.S.; Deb, S.: Cuckoo search via Lévy flights. In: 2009 World Congress on Nature & Biologically Inspired Computing (NaBIC), pp. 210–214. IEEE (2009)

70. Yang, X.S.; Deb, S.: Engineering optimisation by cuckoo search. Int. J. Math. Model. Numer. Optim. **1**(4), 330–343 (2010)

71. Mohamad, A.B.; Zain, A.M.; NaziraBazin, N.E.: Cuckoo search algorithm for optimization problems—a literature review and its applications. Appl. Artif. Intell. **28**(5), 419–448 (2014)

72. Chiroma, H.; Herawan, T.; Fister Jr., I.; Fister, I.; Abdulkareem, S.; Shuib, L.; Hamza, M.F.; Saadi, Y.; Abubakar, A.: Bio-inspired computation: recent development on the modifications of the cuckoo search algorithm. Appl. Soft Comput. **61**, 149–173 (2017)